Ma, C., Marsh, J., Lodge, R.W.D., and Sherlock, R., 2022, Crustal growth/reworking and stabilization of the western Superior Province: Insights from a Neoarchean gneiss complex of the Winnipeg River terrane: GSA Bulletin, https://doi.org/10.1130/B36441.1.

Supplemental Material

Figure S1. Representative photomicrographs of all the samples in the study. The photomicrographs of samples MEST19CMA0009A-G02 and MEST19CMA0007C-G01 were taken with plane-polarized light whereas the others were taken with cross-polarized light.

Figure S2. (A) FeOt/(FeOt + MgO) versus weight percent SiO_2. (B) Modified alkali-lime index diagram. (C) Aluminum saturation index diagram. After Frost et al. (2001).

Figure S3. U-Pb data, zircon cathodoluminescence images, and outcrop of the remaining samples (sample #3 is not plotted due to large number of discordant or Pb loss analyses).

Figure S4. Assessment of zircon trace element data for post-crystallization alternation and undetected mineral inclusions (A) and for effects of alteration on $^{207}Pb/^{206}Pb$ ages (B) and Hf data (C). All the zircon that passed the age filters are included.

Figure S5. Representative trace element data of zircon as in main text Figure 10 but including the limited >3000 Ma zircon. See main text Figure 10 for descriptions.

Figure S6. Concordia diagram showing U-Pb analyses for zircon reference materials DD91-1 and Maniitsoq.

Figure S7. Initial $^{176}Hf/^{177}Hf$ measured for zircon reference materials 91500, FC1, OG1, MUN1 and MUN3

Figure S8. $^{178}Hf/^{177}Hf$ measured for zircon reference materials 91500, FC1, OG1, MUN1 and MUN3.

Text. LA-ICP-MS analytical methods

Table S1. Whole-rock major and trace element data.

Table S2. Zircon U-Pb, trace element, and Lu-Hf data.

Table S3. Neptune Plus MC-ICP-MS Faraday cup configuration for U-Pb and Hf isotope analyses.

Table S4. Analytical set-up for zircon U-Pb, trace element, and Hf analyses.

SUPPLEMENTARY FILE:

Crustal growth/reworking and the stabilization of the western Superior Province: Insights from a Neoarchean gneiss complex of the Winnipeg River terrane

Chong Ma[1, *], Jeffrey Marsh[1], Robert W. D. Lodge[2], Ross Sherlock[1]

1. *Mineral Exploration Research Centre, Harquail School of Earth Science, Laurentian University, Sudbury, Ontario, Canada P3E2C6*
2. *Department of Geology, University of Wisconsin-Eau Claire, Eau Claire, Wisconsin, USA 54702*

* Corresponding author: macmachong@gmail.com

Contents:

- **Supplementary figures (Figure S1–S5)**
- **LA-ICP-MS analytical methods**
- **Supplementary tables (Table S1–S2)**

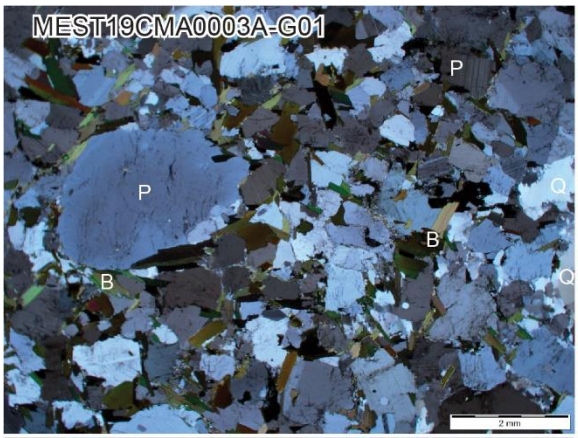
MEST19CMA0003A-G01
P
P
Q
B
B
Q
2 mm

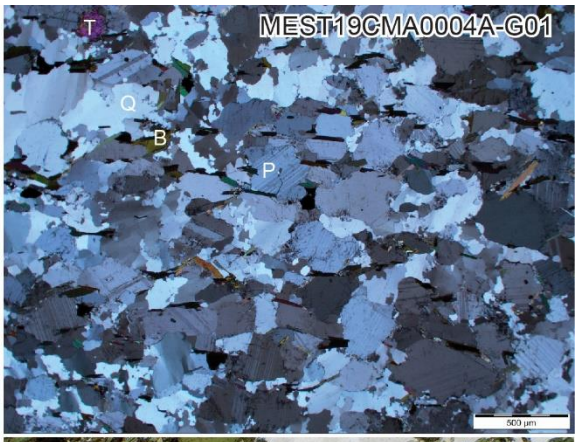
T
MEST19CMA0004A-G01
Q
B
P
500 µm

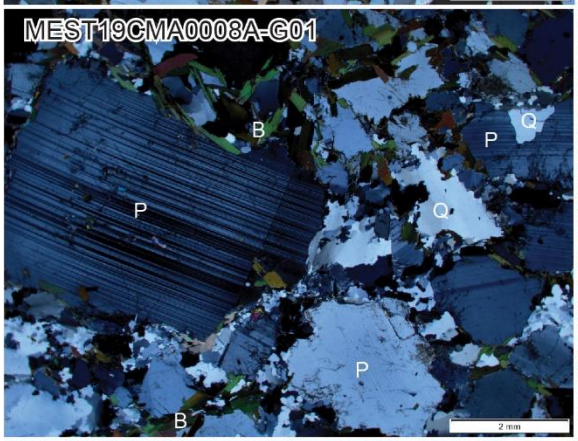
MEST19CMA0008A-G01
B
P
Q
P
Q
P
B
2 mm

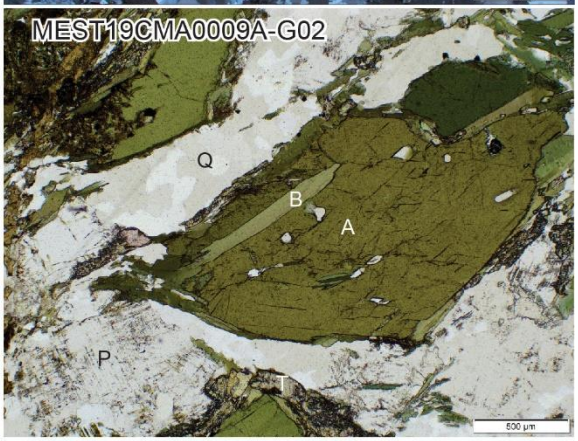
MEST19CMA0009A-G02
Q
B
A
P
T
500 µm

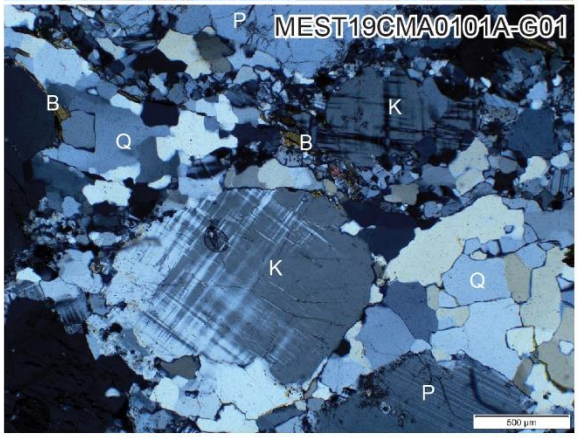
P
MEST19CMA0101A-G01
B
K
Q
B
K
Q
P
500 µm

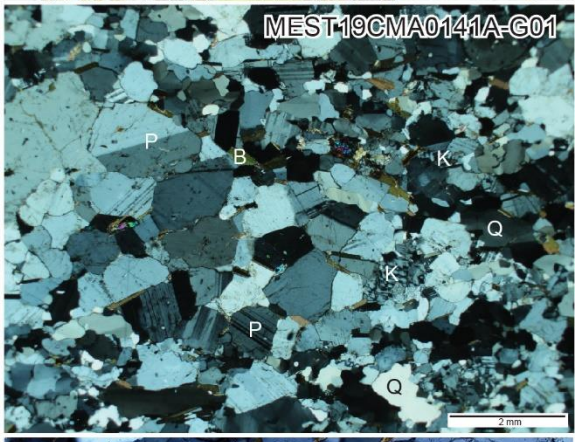
MEST19CMA0141A-G01
P
B
K
Q
K
P
Q
2 mm

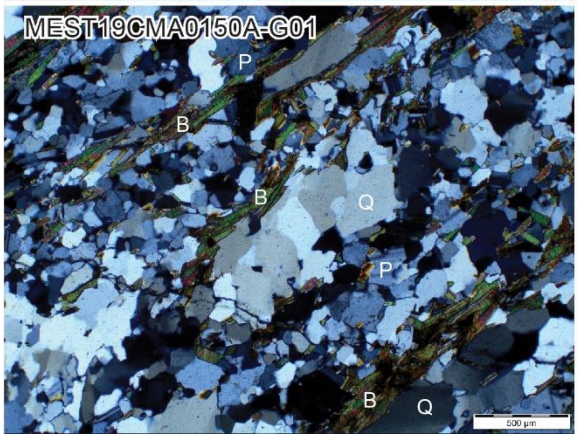
MEST19CMA0150A-G01
P
B
B
Q
P
B
Q
500 µm

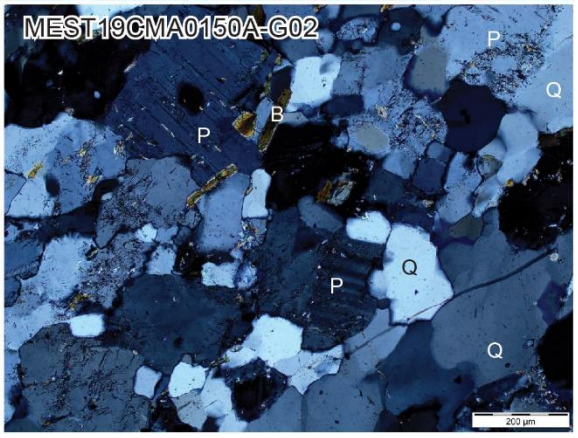
MEST19CMA0150A-G02
P
Q
B
P
Q
P
Q
200 µm

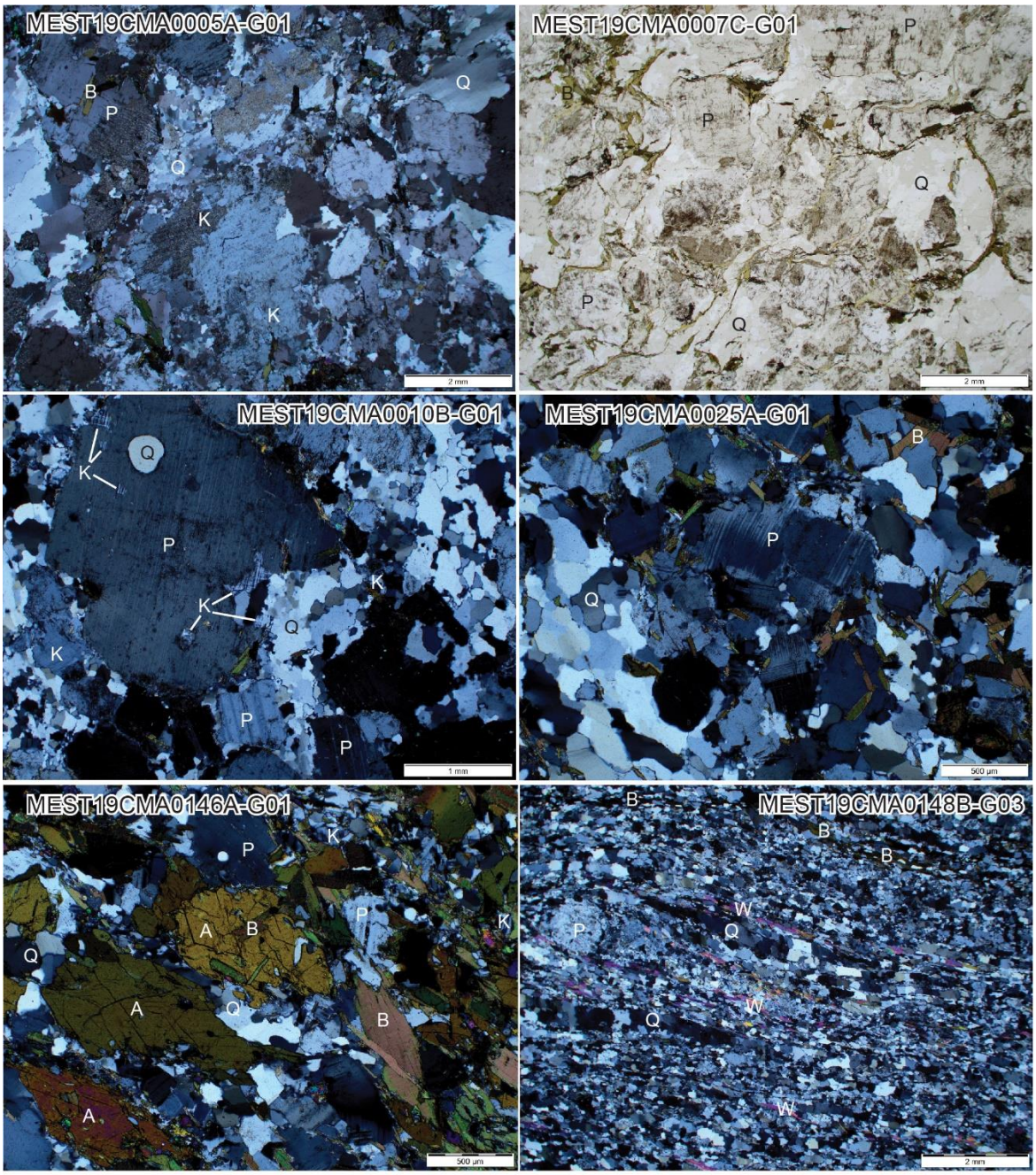

Figure S1. Representative photomicrographs of all the samples in the study. The photomicrographs of samples MEST19CMA0009A-G02 and MEST19CMA0007C-G01 were taken with plane-polarized light whereas the others were taken with cross-polarized light.

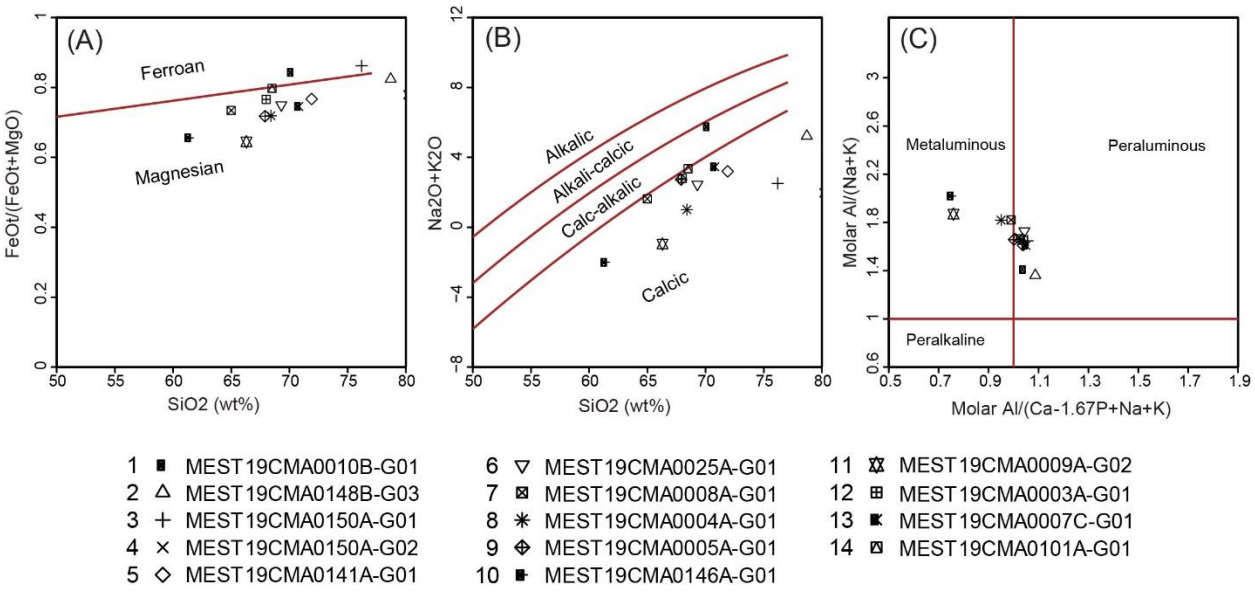

Figure S2. (A) FeO_t/(FeO_t + MgO) versus weight percent SiO_2. (B) Modified alkali-lime index diagram. (C) Aluminum saturation index diagram. After Frost et al. (2001).

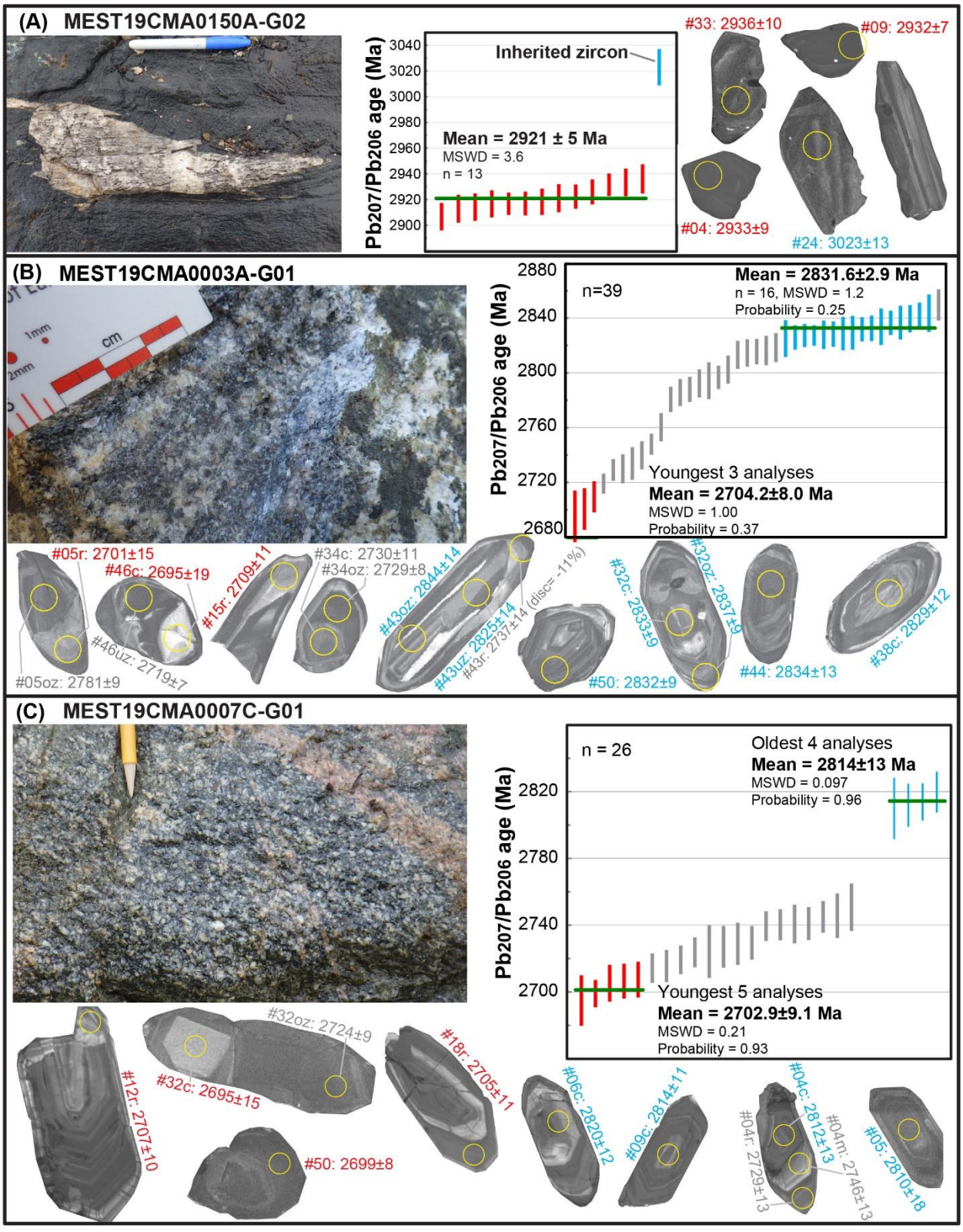
(A) MEST19CMA0150A-G02
Pb207/Pb206 age (Ma)
3040
3020
3000
2980
2960
2940
2920
2900
Inherited zircon
Mean = 2921 ± 5 Ma
MSWD = 3.6
n = 13
#33: 2936±10
#09: 2932±7
#04: 2933±9
#24: 3023±13
(B) MEST19CMA0003A-G01
1mm
cm
2mm
Pb207/Pb206 age (Ma)
2880
2840
2800
2760
2720
2680
n=39
Mean = 2831.6±2.9 Ma
n = 16, MSWD = 1.2
Probability = 0.25
Youngest 3 analyses
Mean = 2704.2±8.0 Ma
MSWD = 1.00
Probability = 0.37
#05r: 2701±15
#46c: 2695±19
#15r: 2709±11
#34c: 2730±11
#34oz: 2729±8
#43oz: 2844±14
#43uz: 2825±14
#43r: 2737±14 (disc= -11%)
#32c: 2833±9
#32oz: 2837±9
#38c: 2829±12
#05oz: 2781±9
#46uz: 2719±7
#50: 2832±9
#44: 2834±13
(C) MEST19CMA0007C-G01
Pb207/Pb206 age (Ma)
2820
2780
2740
2700
n = 26
Oldest 4 analyses
Mean = 2814±13 Ma
MSWD = 0.097
Probability = 0.96
Youngest 5 analyses
Mean = 2702.9±9.1 Ma
MSWD = 0.21
Probability = 0.93
#32oz: 2724±9
#18r: 2705±11
#12r: 2707±10
#32c: 2695±15
#50: 2699±8
#06c: 2820±12
#09c: 2814±11
#04c: 2812±13
#04m: 2746±13
#04r: 2729±13
#05: 2810±18

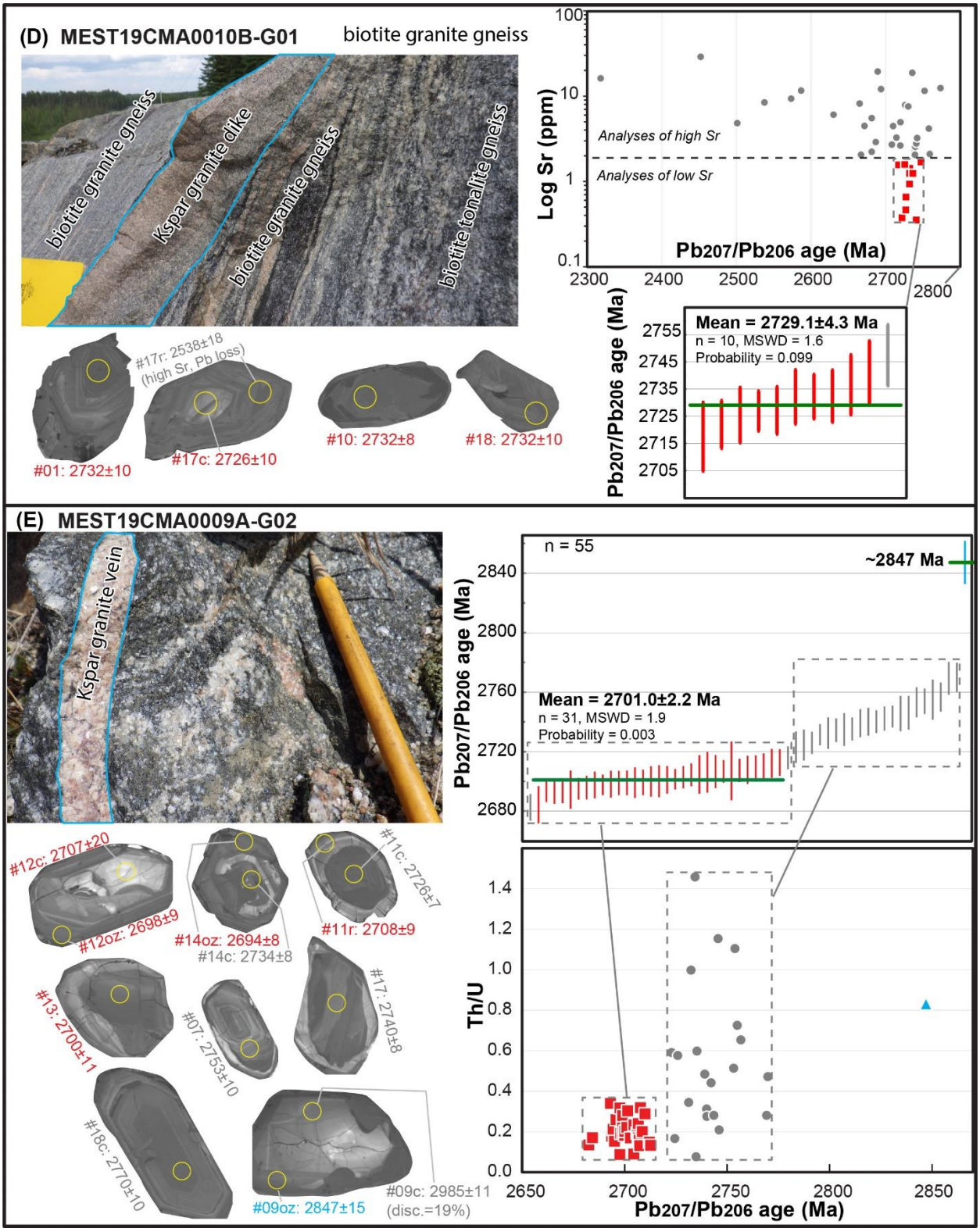

Figure S3. U-Pb data, zircon cathodoluminescence images, and outcrop of the remaining samples (sample #3 is not plotted due to large number of discordant or Pb loss analyses).

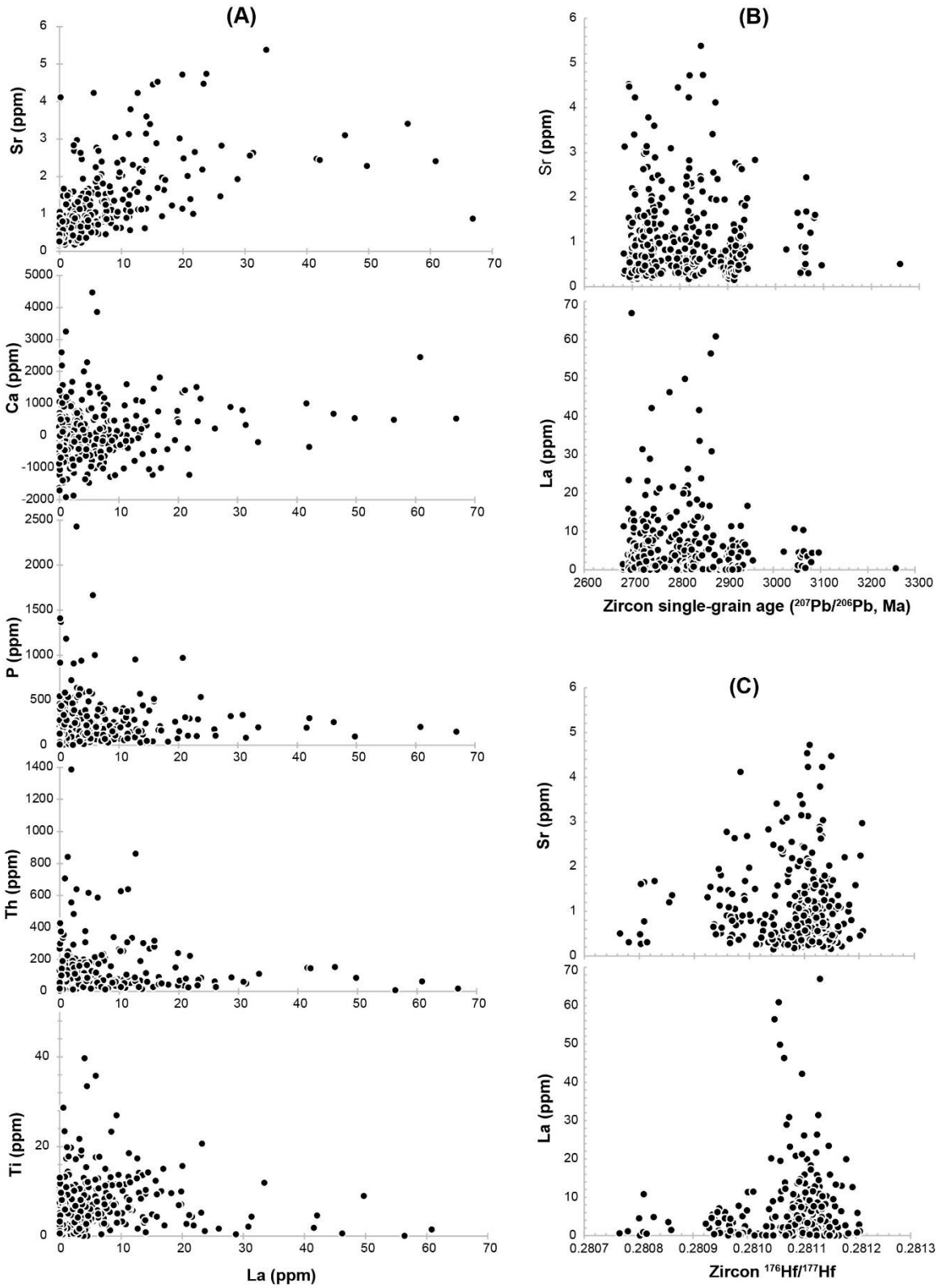

Figure S4. Assessment of zircon trace element data for post-crystallization alternation and undetected mineral inclusions (A) and for effects of alteration on $^{207}Pb/^{206}Pb$ ages (B) and Hf data (C). All the zircon that passed the age filters are included.

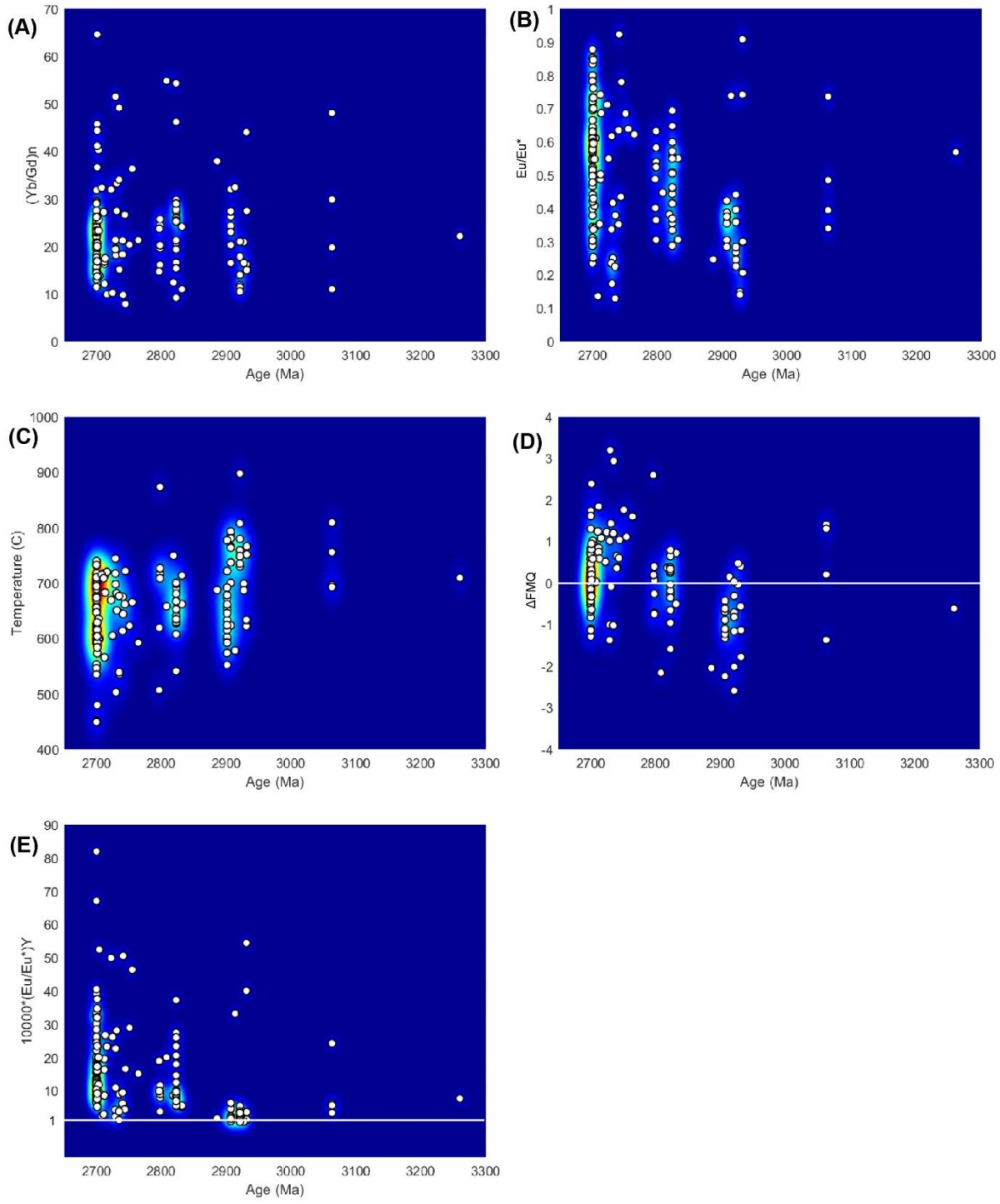

Figure S5. Representative trace element data of zircon as in main text Figure 10 but including the limited >3000 Ma zircon. See main text Figure 10 for descriptions.

LA-ICP-MS analytical methods

Zircon U-Th-Pb, trace element (TE), and Hf isotope analyses were conducted at the Mineral Exploration Research Centre - Isotope Geochemistry Lab (MERC-IGL), at Laurentian University. Laser ablation sampling was performed using a Photon Machines Analyte G2 ArF excimer laser, with 193 nm wavelength, <5 ns pulse width, and HelEx II cell. U-Th-Pb and Hf isotope measurements were conducted using a Thermo Scientific Neptune Plus multicollector (MC) ICP-MS, equipped with Jet interface and nine Faraday cups. The cup configuration for U-Pb and Hf isotope analyses is shown in Table S3. All MC-ICP-MS analyses were conducted in low resolution, static mode to ensure maximum sensitivity and stability. TE measurements were conducted using a Thermo Scientific iCap-TQ ICP-MS in single quad mode to ensure maximum sensitivity on the low to intermediate mass range.

Table S3. Neptune Plus MC-ICP-MS Faraday cup configuration for U-Pb and Hf isotope analyses.

	L4	L3	L2	L1	C	H1	H2	H3	H4
U-Th-Pb	204Pb	206Pb	207Pb	208Pb	~220.65		232Th		238U
Hf	171Yb	173Yb	174Hf	175Lu	176Yb, Lu/Hf	177Hf	178Hf	179Hf	

U-Th-Pb and trace element analytical setup

U-Th-Pb and TE measurements were conducted simultaneously on the Neptune Plus and iCap-TQ, respectively, by splitting the ablated aerosol downstream of the sample cell (LASS; e.g., Kylander-Clark et al., 2013). Helium carrier gas flows through the ablation cell were 0. 7 l/min (cup) and 0.05 l/min (cell), with 1.16 l/min Ar and 13 ml/min N_2 makeup gas added downstream of the cell. Ablation spot diameter was 25 μm, with 30 second duration, laser fluence of 3 J/cm^2, and 7 Hz repetition rate, leaving estimated ablation pit depths of <15 μm. Sixty seconds of background were measured at the beginning and end of the analytical session, with 30 seconds of background measured between each ablation.

For U-Th-Pb isotope analysis on the Neptune Plus, the ~15% Faraday cup mass range allows isotopes between ^{204}Hg/Pb to ^{238}U to be measured simultaneously, with the cup configuration shown in Table S3 and fictive mass of ~220.60 aligned with the center cup. All cups were coupled with 10^{11} Ω amplifiers, with the exception of L2, which was coupled with 10^{12} Ω amplifier for better precision on the low intensity ^{207}Pb signal. Ion beam drift from day to day was typically <0.05amu, with flat top peak width typically ~0.2 amu, ensuring stable on-peak measurements throughout long-duration analytical sessions. Cool gas flows and RF power were set at 16 L/min and 1200 W, with Ar auxiliary gas flow of 0.75 L/min and makeup gas flows between 0.38 l/min.

For trace element analysis on the iCap-TQ, the masses measured and associated dwell times are shown in Table S4. Cool gas, auxiliary gas, and RF power were set at 14 L/min, 0.8 L/min, and 1550 W, respectively, with Ar makeup gas flow of 0.1 l/min. Extraction lens and quadrupole entry lens voltages were tuned to maximize sensitivity in the low mass range, to compensate for the generally poorer low mass transmission.

The raw U-Th-Pb and TE data were synchronized in Iolite v.4, along with the laser log file, prior to processing, so that the same timeslices (selections) for each analysis were used in the calculations. Baseline subtraction, instrumental drift, and downhole fractionation corrections were performed with the U-Pb Geochronology data reduction scheme (DRS) implemented within Iolite v.4 (Paton et al., 2011; Petrus and Kamber, 2012), with U-Th-Pb isotope ratios normalized to the zircon reference material (RM) OGC (OG1; 3465 ± 1 Ma; Stern et al., 2009). OCG was analyzed three times at the beginning and end of each session, and once every ten unknowns throughout the session (~60-80 total analyses). Four seconds at the beginning and one second at end of the ablation period were excluded from the selections in order to minimize potential fractionation effects, leaving ~25 seconds of signal for integration. Within run variance in the measured ratios for OGC (i.e., the additional percent error required to achieve MSWD = 1) was propagated into the 2SE uncertainty for all unknowns. No additional uncertainty propagation was applied to the $^{207}Pb/^{206}Pb$ ratios of unknown analyses, due to the long-term variance of $^{207}Pb/^{206}Pb$ ratios of verification RMs run at the MERC-IGL having MSWD < 1 (e.g., Horstwood et al., 2016). Two verification RMs were analyzed during the session to ensure accuracy of the U-Pb ratios. Across all sessions DD91-1 (TIMS age = 2682 ± 1 Ma; Davis, 2002) yielded an intercept age of 2681 ± 2.1 Ma (MSWD = 0.91) and Maniitsoq (TIMS age = 3008.9 ± 0.72 Ma; Marsh et al., 2019) yielded an intercept age of 3008.5 ± 1.9 Ma (MSWD = 0.62; Fig. S6). Trace element data were processed using the Internal Standard DRS within Iolite v4, and normalized to the synthetic glass NIST610 RM. An assumed stoichiometric concentration of 15.284 wt% Si was used for all zircon, to account for differing ablation characteristics between the glass and zircon. The synthetic glass NIST612 and zircon RM 91500 were used to verify the accuracy of TE analysis (within the range of published values; Table S4).

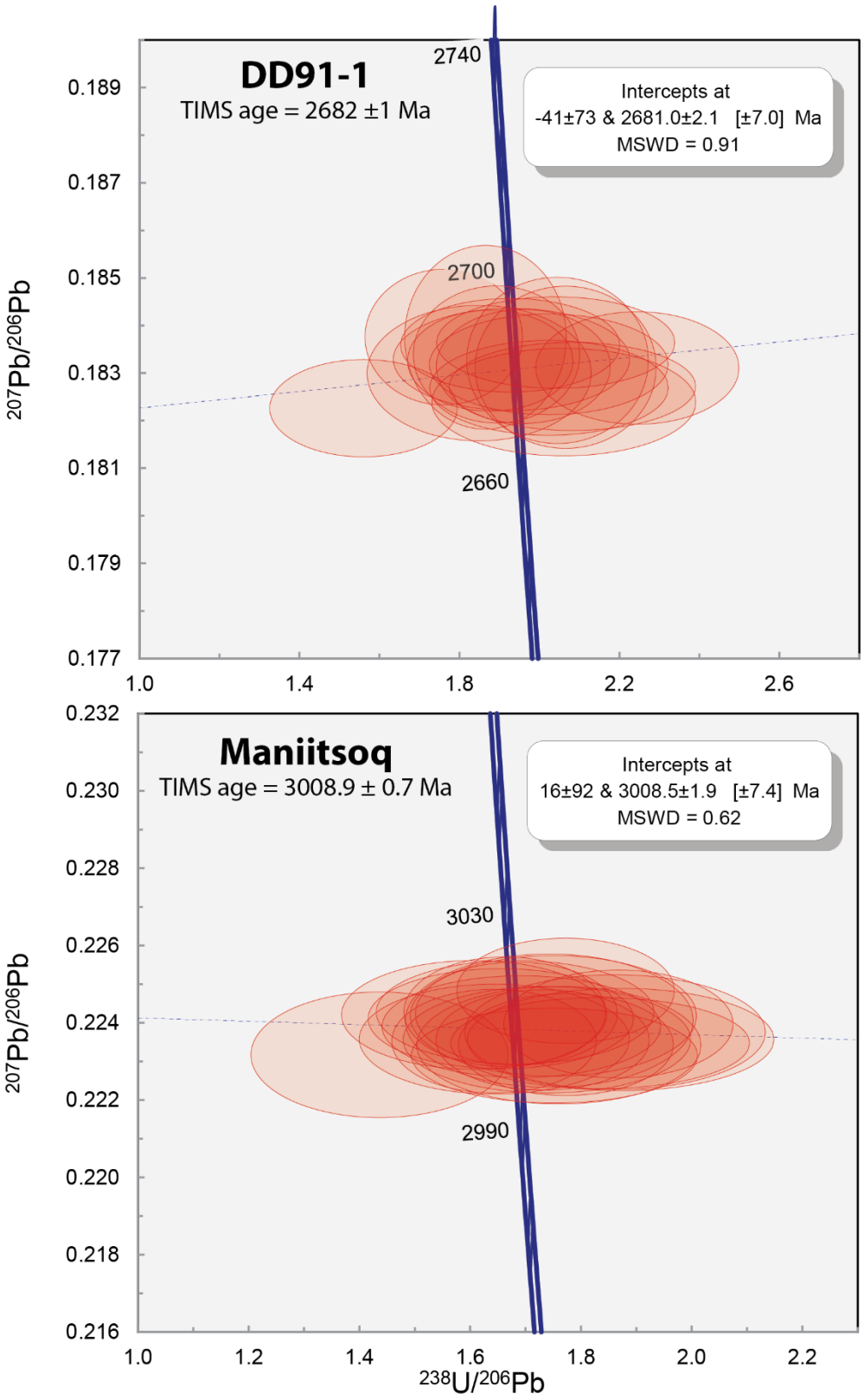

Figure S6. Concordia diagram showing U-Pb analyses for zircon reference materials DD91-1 and Maniitsoq.

Hf isotope analytical setup

Hf isotope measurements were conducted in the same spot locations following U-Th-Pb and TE LASS analysis with the ablated aerosol stream directed solely to the Neptune Plus in order to achieve maximum signal intensity and internal precision. Helium carrier gas flow through the ablation cell was 0.625 l/min (cup) and 0.05 l/min (cell), with 0.7 l/min Ar and 8 ml/min N_2 makeup gas added downstream of the cell. An ablation spot diameter of 40 μm, with ablation duration of 60 seconds, laser fluence of 6 J/cm^2, and 7 Hz repetition rate, leaving estimated ablation pit depths of ~30 μm. Sixty seconds of background were measured the beginning and end of the analytical session, with 30 seconds of background measured between each ablation.

The cup configuration for Hf isotope analysis on the Neptune Plus is shown in Table S3, and all cups were coupled with 10^{11} Ω amplifiers. Ion beam drift from day to day was typically <0.05 amu, with flat top peak width typically >0.175 amu, ensuring stable on-peak measurements throughout long-duration analytical sessions. Cool gas flows and RF power were set at 16 L/min and 1200 W, with Ar auxiliary gas flow of 0.8 L/min and makeup gas flow of 0.05 l/min.

The raw Hf isotope data were processed in Iolite v4, with baseline subtraction, instrumental drift, and mass bias corrections performed with a customized version of the Hf Isotope DRS (see below). Isotope ratios were normalized to the zircon RM Plesovice (337.3 ± 0.4 Ma; $^{176}Hf/^{177}Hf$ = 0.282482; Sláma et al., 2008). Instrumental mass bias and interference correction factors for ^{176}Yb and ^{176}Lu were determined within the session through iterative calculation of the effective $^{176}Yb/^{173}Yb$ ratio required to yield identical $^{176}Hf/^{177}Hf$ ratios for the variably HREE-doped MUN synthetic zircon (MUN1 = ~400 ppm Yb; MUN3 = ~1400 ppm Yb; $^{176}Hf/^{177}Hf$ = 0.282135 ± 7 Fisher et al., 2011). The effective (mass bias corrected) within session $^{176}Yb/^{173}Yb$ was then applied in the interference correction for all analyses as part of the DRS. Hafnium mass bias was corrected using the natural $^{179}Hf/^{177}Hf$ of 0.7325 (Stevenson and Patchett, 1990).

Plesovice was analyzed three times at the beginning and end of each session, and once every ten unknowns throughout the session. Three seconds at the beginning and two seconds at the end of the ablation period were excluded from the selections in order to minimize potential fractionation effects, leaving 55 seconds of signal for integration. Within run variance in the measured $^{176}Hf/^{177}Hf$ ratios for Plesovice was propagated into the 2SE uncertainty for all unknowns as part of the DRS. No additional uncertainty propagation was applied to the Hf isotope ratios of unknown analyses, due to the long-term variance of measured $^{176}Hf/^{177}Hf$ ratios for verification RMs across all sessions having MSWD < 1. Five verification RMs were analyzed during the session to ensure accuracy of the Hf isotope ratios and efficacy of the mass bias and interference corrections, with the initial $^{176}Hf/^{177}Hf$ values for virtually all RM analyses within uncertainty of the published values. The efficacy of the mass bias and interference corrections is demonstrated by the lack of sensitivity of the $^{176}Hf/^{177}Hf$ ratios across the

range of Yb/Hf (Fig. S7; Table S4). The mean $^{178}Hf/^{177}Hf$ values for all RMs were within uncertainty of the natural value of 1.46717 (Fig. S8).

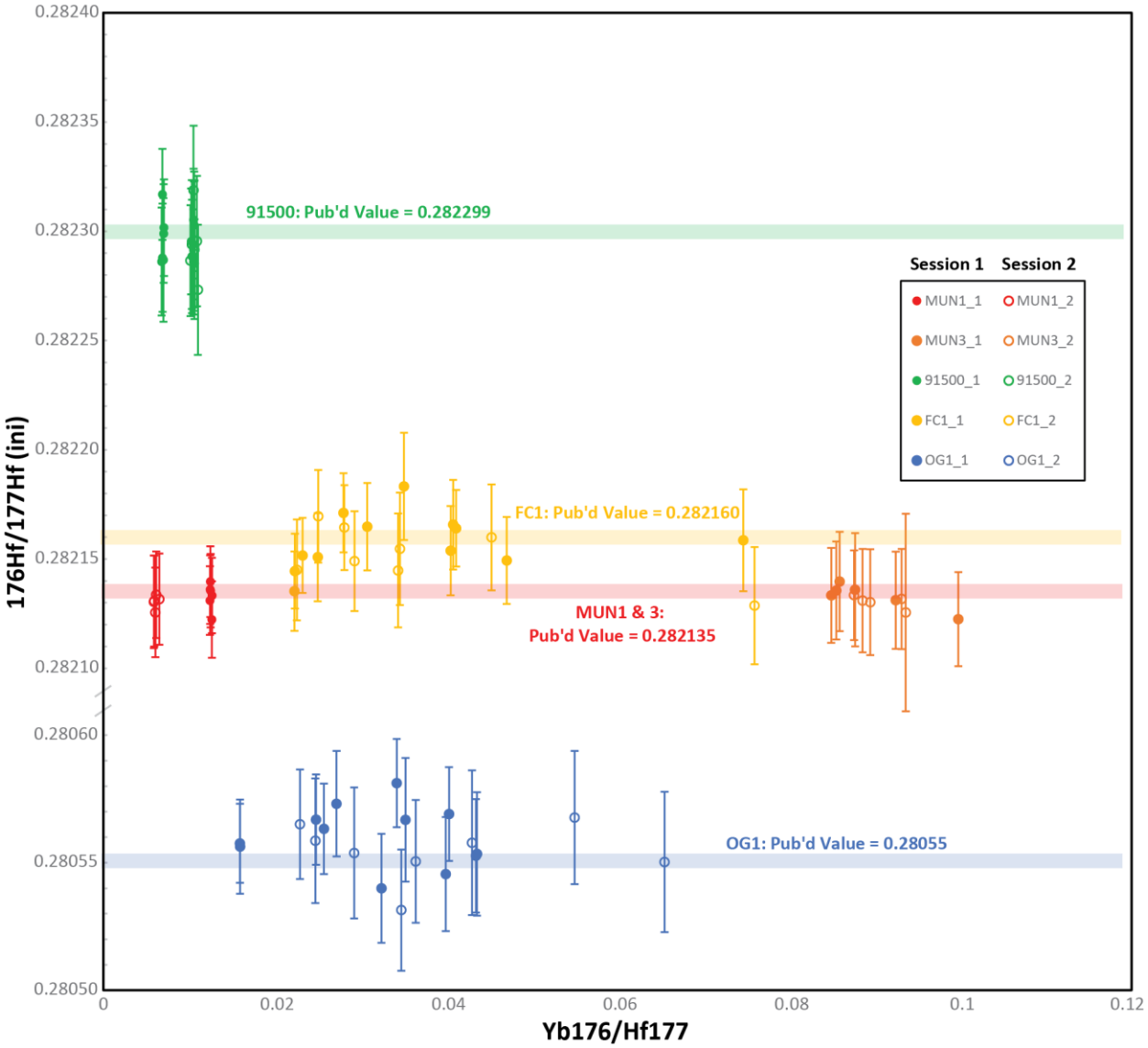

Figure S7. Initial $^{176}Hf/^{177}Hf$ measured for zircon reference materials 91500, FC1, OG1, MUN1 and MUN3

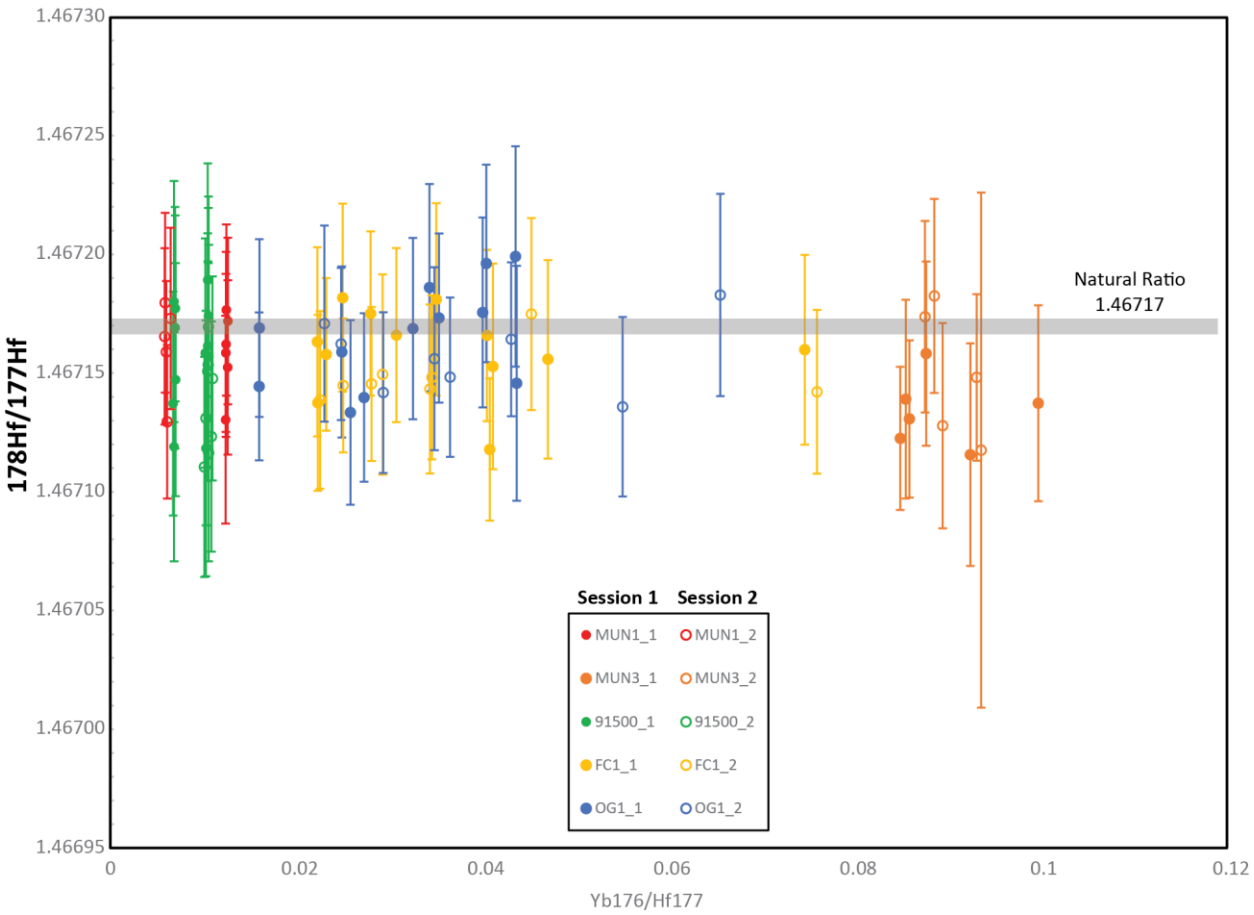

Figure S8. $^{178}Hf/^{177}Hf$ measured for zircon reference materials 91500, FC1, OG1, MUN1 and MUN3.

Table S4. Analytical set-up for zircon U-Pb, trace element, and Hf analyses.

U-Pb:

Laboratory & Sample Preparation	
Laboratory name	MERC IGL
Sample type/mineral	Zircon
Analysis	U-Pb
Sample preparation	polished mount
Reference material location	Separate mount
Imaging	CL
Laser ablation system	
Make, Model & type	Photon Machines, Analyte G2
Ablation cell & volume	Helex II, large format, two volume
Laser wavelength (nm)	193

Pulse width (ns)	<4
Fluence (J.cm-2)	3
Repetition rate (Hz)	7
Ablation duration (secs)	30
Ablation pit depth / ablation rate	~15 um/ ~0.5 um/sec
Spot size (um)	25
Sampling mode / pattern	spot
Carrier gas	He & Ar (after cell) & N2 (after cell)
Cell carrier gas flow (l/min)	He1 (cup) = 0.7, He2 (cell) = 0.05, Ar = 1.54, N2 = 0.013
ICP-MS Instrument	
Make, Model & type	Thermo Neptune Plus with Jet Interface
Sample introduction	Laser Ablation
RF power (W)	1200
Make-up gas flow (l/min)	0.07
Detection system	9 Faraday Cups
Masses measured	204, 206, 207, 208, 232, 238
Integration time per peak/dwell times (ms)	NA
Total integration time per output datapoint (secs)	0.25
'Sensitivity' as useful yield (%, element)	
IC Dead time (ns)	NA
Data Processing	
Gas blank	Measured for 90 sec at beginning and end of run & 30 sec between ablations
Calibration strategy	Standard Sample bracketing
Reference Material info	Primary RM = OG1 (3465.4 ± 0.6 Ma; Stern et al., 2009), Secondary RMs = DM18-1 (2678-2682 Ma; Davis (2002)), and Maniitsoq (Grn; 3008.7 ± 0.72 Ma; Marsh et al., 2019))
Data processing package used / Correction for LIEF Mass discrimination	Iolite v. 4; DRS = U-Pb Geochron
Common-Pb correction, composition and uncertainty	NA
Uncertainty level & propagation	Spots = 2SE, Wtd. Means = 2 SD with propagation of in-run variance in primary RM
Quality control / Validation	DM18-1 = 2681 ± 2.1 Ma; Grn = 3008.5 ± 1.9 Ma (207Pb/206Pb Wtd. Means; n = 20)

Trace Element:

Laboratory & Sample Preparation	
Laboratory name	MERC IGL
Sample type/mineral	Zircon
Sample preparation	polished mount
Reference material location	separate mount
Imaging	CL
Laser ablation system	
Make, Model & type	Photon Machines, Analyte G2
Ablation cell & volume	Helex II, large format, two volume
Laser wavelength (nm)	193

Pulse width (ns)	<4
Fluence (J.cm-2)	6
Repetition rate (Hz)	7
Ablation duration (secs)	60
Ablation pit depth / ablation rate	~30 um/ ~0.5 um/sec
Spot size (um)	40
Sampling mode / pattern	spot
Carrier gas	He & Ar (after cell) & N2 (after cell)
Cell carrier gas flow (l/min)	He1 (cup) = 0.625, He2 (cell) = 0.05, Ar = 0.7, N2 = 0.008
ICP-MS Instrument	
Make, Model & type	Thermo Neptune Plus with Jet Interface
Sample introduction	Laser Ablation
RF power (W)	1200
Make-up gas flow (l/min)	0.07
Detection system	9 Faraday Cups
Masses measured	171, 173, 174, 175, 176, 177, 178, 179
Integration time per peak/dwell times (ms)	NA
Total integration time per output datapoint (secs)	1.049
'Sensitivity' as useful yield (%, element)	
IC Dead time (ns)	NA
Data Processing	
Gas blank	Measured for 60 sec at beginning and end of run & 30 sec between ablations
Calibration strategy	Standard Sample bracketing
Reference Material info	Primary RM = Plesovice (176/177Hf = 0.282482; Sláma et al., 2008), Secondary RMs = 91500 (176/177Hf = 0.282306; 176/177Hfi = 0.282299; Woodhead and Hergt, 2005), FC1 (176/177Hf = 0.282184; 176/177Hfi = 0.282157; Woodhead and Hergt, 2005), OGC (176/177Hf = 0.280633; 176/177Hfi = 0.28055; Stern et al., 2009); (MUN1/3 (176/177Hf = 0.282135; Fisher et al., 2011)
Data processing package used / Correction for LIEF Mass discrimination	Iolite v. 4; DRS = Hf isotopes
Common-Pb correction, composition and uncertainty	NA
Uncertainty level & propagation	Spots = 2SE, Wtd. Means = 2 SD with propagation of in-run variance in primary RM
Quality control / Validation	91500 = 0.282295 (22), FC1 = 0.282155 (26), OG1 = 0.280558 (23), MUN 1 & 3= 0.282132 (10) (Interference, Mass Bias, and Age corrected 176/177Hf)

Hf:

Laboratory & Sample Preparation	
Laboratory name	MERC IGL
Sample type/mineral	Zircon
Sample preparation	polished mount
Reference material location	separate mount
Imaging	CL

Laser ablation system	
Make, Model & type	Photon Machines, Analyte G2
Ablation cell & volume	Helex II, large format, two volume
Laser wavelength (nm)	193
Pulse width (ns)	<4
Fluence (J.cm-2)	6
Repetition rate (Hz)	7
Ablation duration (secs)	60
Ablation pit depth / ablation rate	~30 um/ ~0.5 um/sec
Spot size (um)	40
Sampling mode / pattern	spot
Carrier gas	He & Ar (after cell) & N2 (after cell)
Cell carrier gas flow (l/min)	He1 (cup) = 0.625, He2 (cell) = 0.05, Ar = 0.7, N2 = 0.008
ICP-MS Instrument	
Make, Model & type	Thermo Neptune Plus with Jet Interface
Sample introduction	Laser Ablation
RF power (W)	1200
Make-up gas flow (l/min)	0.07
Detection system	9 Faraday Cups
Masses measured	171, 173, 174, 175, 176, 177, 178, 179
Integration time per peak/dwell times (ms)	NA
Total integration time per output datapoint (secs)	1.049
'Sensitivity' as useful yield (%, element)	
IC Dead time (ns)	NA
Data Processing	
Gas blank	Measured for 60 sec at beginning and end of run & 30 sec between ablations
Calibration strategy	Standard Sample bracketing
Reference Material info	Primary RM = Plesovice (176/177Hf = 0.282482; Sláma et al., 2008), Secondary RMs = 91500 (176/177Hf = 0.282306; 176/177Hfi = 0.282299; Woodhead and Hergt, 2005), FC1 (176/177Hf = 0.282184; 176/177Hfi = 0.282157; Woodhead and Hergt, 2005), OGC (176/177Hf = 0.280633; 176/177Hfi = 0.28055; Stern et al., 2009); (MUN1/3 (176/177Hf = 0.282135; Fisher et al., 2011)
Data processing package used / Correction for LIEF	Iolite v. 4; DRS = Hf isotopes
Mass discrimination	
Common-Pb correction, composition and uncertainty	NA
Uncertainty level & propagation	Spots = 2SE, Wtd. Means = 2 SD with propagation of in-run variance in primary RM
Quality control / Validation	91500 = 0.282295 (22), FC1 = 0.282155 (26), OG1 = 0.280558 (23), MUN 1 & 3= 0.282132 (10) (Interference, Mass Bias, and Age corrected 176/177Hf)

Supplementary tables (see the Excel files):

Table S1. Whole-rock major and trace element data.

Table S2. Zircon U-Pb, trace element, and Lu-Hf data.

References:

Davis, D.W. (2002) U–Pb geochronology of Archean metasedimentary rocks in the Pontiac and Abitibi subprovinces, Quebec, constraints on timing, provenance and regional tectonics. Precambrian Research 115, 97-117.

Fisher, C.M., Hanchar, J.M., Samson, S.D., Dhuime, B., Blichert-Toft, J., Vervoort, J.D. and Lam, R. (2011) Synthetic zircon doped with hafnium and rare earth elements: A reference material for in situ hafnium isotope analysis. Chemical Geology 286, 32-47.

Frost, B.R., Barnes, C.G., Collins, W.J., Arculus, R.J., Ellis, D.J., and Frost, C.D. (2001) A geochemical classification for granitic rocks: Journal of Petrology 42, 2033-2048, https://doi .org/10.1093/petrology/42.11.2033.

Horstwood, M.S., Košler, J., Gehrels, G., Jackson, S.E., McLean, N.M., Paton, C., Pearson, N.J., Sircombe, K., Sylvester, P. and Vermeesch, P. (2016) Community-derived standards for LA-ICP-MS U-(Th-) Pb geochronology–Uncertainty propagation, age interpretation and data reporting. Geostandards and Geoanalytical Research 40, 311-332.

Kylander-Clark, A.R., Hacker, B.R. and Cottle, J.M. (2013) Laser-ablation split-stream ICP petrochronology. Chemical Geology 345, 99-112.

Marsh, J.H., Joergensen, T., Petrus, J.A., Hamilton, M. and Mole, D.M. (2019) U-Pb, trace element, and hafnium isotope composition of the Maniitsoq zircon: A potential new Archean zircon reference material, Goldschmidt, Barcelona, Spain.

Paton, C., Hellstrom, J., Paul, B., Woodhead, J. and Hergt, J. (2011) Iolite: Freeware for the visualisation and processing of mass spectrometric data. Journal of Analytical Atomic Spectrometry 26, 2508-2518.

Paton, C., Woodhead, J.D., Hellstrom, J.C., Hergt, J.M., Greig, A. and Maas, R. (2010) Improved laser ablation U-Pb zircon geochronology through robust downhole fractionation correction. Geochemistry, Geophysics, Geosystems 11 (3).

Sláma, J., Košler, J., Condon, D.J., Crowley, J.L., Gerdes, A., Hanchar, J.M., Horstwood, M.S., Morris, G.A., Nasdala, L. and Norberg, N. (2008) Plešovice zircon—a new natural reference material for U–Pb and Hf isotopic microanalysis. Chemical Geology 249, 1-35.

Stern, R.A., Bodorkos, S., Kamo, S.L., Hickman, A.H. and Corfu, F. (2009) Measurement of SIMS Instrumental Mass Fractionation of Pb Isotopes During Zircon Dating. Geostandards and Geoanalytical Research 33, 145-168.

Stevenson, R.K. and Patchett, P.J. (1990) Implications for the evolution of continental crust from Hf isotope systematics of Archean detrital zircons. Geochimica et Cosmochimica Acta 54, 1683-1697.

Wiedenbeck, M., Alle, P., Corfu, F., Griffin, W., Meier, M., Oberli, F.v., Quadt, A.v., Roddick, J. and Spiegel, W. (1995) Three natural zircon standards for U-Th-Pb, Lu-Hf, trace element and REE analyses. Geostandards newsletter 19, 1-23.

Wiedenbeck, M., Hanchar, J.M., Peck, W.H., Sylvester, P., Valley, J., Whitehouse, M., Kronz, A., Morishita, Y., Nasdala, L. and Fiebig, J. (2004) Further characterisation of the 91500 zircon crystal. Geostandards and Geoanalytical Research 28, 9-39.

Woodhead, J.D. and Hergt, J.M. (2005) A preliminary appraisal of seven natural zircon reference materials for in situ Hf isotope determination: Geostandards and Geoanalytical Research 29, 183-195.